An Investigation of the Strength and Stiffness of Weight-Saving Sandwich Beams with CFRP face sheets and Seven 3D Printed Cores

Ahmad W. Alshaer* and Daniel J. Harland

School of Engineering, University of Central Lancashire, Fylde Road, Preston, PR1 2HE, The United Kingdom

Abstract

Although sandwich panels are widely used in the industry, the limitations in the cores' structure designs and materials restrain their use in stiffness- or strength-critical applications without increasing the sandwich beams' dimensions. The use of additive manufacturing over conventional fabrication methods enabled us to tune the cores' design according to the stiffness and strength requirements without increasing the beams' overall dimensions. Seven core structures were 3D printed of Nylon PA12 using powder bed fusion and were tested for their strength and stiffness using three-point bending test. The novel 3D printed core structures were combined, for the first time in the literature, with thin CFRP face sheets. The small Re-entrant and Gyroid structures achieved the highest strength and stiffness values respectively, while the 3D printed conventional honeycomb structures performed the poorest among all other core structures. The stiffness and strength values were normalised using the samples weights and the gyroid structure recorded the highest specific stiffness and strength, making it ideal for supporting weight-critical applications such as motorsport and aerospace.

Keywords

3D Printed Core, Sandwich Beam, Three-Point Bending, Nylon, Powder Bed Fusion.

1. Introduction

In structural engineering, sandwich composite materials are widely used in weight-critical applications in motorsports and aerospace industries where foam has been an ideal feature for forming sandwich cores [1]. These materials, however, show a significant deformation under bending and can be limited when scaled. As a result, researchers developed alternative materials with better mechanical properties including cellular auxetic structures such as hexagonal and re-entrant honeycomb cores and lattice truss structures etc [2].

Several studies, both experimental and numerical, highlighted the superiority of those structures over conventional foam sandwiches in terms of their bending, buckling and impact resistance [3-7]. Despite that, the improvement in the mechanical properties was achieved on the expense of the sandwich weight which increased due to enlarging the cell's dimensions and the need for thicker skin sheets required for the stiffness [8]. Such limitations then pave a path for complex structures with better performance to be additively manufactured and to overcome traditional manufacturing methods limitations such as extrusion, forming and corrugation [9, 10].

Using 3D printing, the compressive resistance of a continuous fibre corrugated structure was investigated using a Kevlar fibre reinforced PLA [11]. Although a good compressive strength of 17 MPa was recorded, only one type of composites was tested using a relatively small-scale sample of 60×60 mm^2 in size. In a different work, Dikshit et al. [12] used inkjet 3D printing to produce two vertical pillared corrugated cores which were fabricated using 80% ABS and 20% flexible rubber with two Kevlar-Nylon face sheets. Higher compressive strength and modulus were recorded for the vertical pillared sine wave corrugation in comparison to the vertical pillared trapezoidal corrugation structures. Although the use of reinforced composites may offer a better compressive strength compared to traditional 3D printed

* Corresponding author. Tel.: +44 (0) 1772 89 3279.
Email: awalshaer@uclan.ac.uk or ahmad_sh1986@yahoo.com

thermoplastic components, the process control and optimisation usually take long time and may be challenging for some structures, and fibre-related defects such as misalignment may jeopardise the components strength and integrity. Moreover, only the compressive strength was evaluated in this research.

Material extrusion was used by Sarvestani et al. [13] to produce PLA hexagonal and auxetic cores structures designed for low-velocity impact applications while the compression resistance of similar 3D printed structures was evaluated in other research [14, 15]. Although good compression resistance was reported, tests were only limited to compression and the samples' small size, containing only a few unit-cells, does not provide a true representation of the behaviour of the beam if they were made of larger sizes or they need to support a long span. Therefore, it is vital to investigate the sandwich beams' behaviour using similar sample sizes to that used in real-life situations. Besides, PLA, used in [13] for instance, is considered a stiff material compared to rubber or nylon that may be more suited for impact absorption applications. In a related investigation conducted by Li T. and Wang L. [16], the bending strength of three acrylic-based photopolymer cores were analysed, namely: honeycomb, re-entrant and the truss. Besides the fact that the authors only tested simple designs that do not require 3D printing for their manufacture, the samples' stiffness values (2.6 to 33 N/mm) were deemed to be poor to support most of the industrial applications. Moreover, since the Verowhite material's properties degrade when operating above 50°C temperature, the sandwiches structure made of such material becomes unstable above this temperature and becomes unsuitable to serve in motorsports and aerospace applications in which the beams are required to operate near the engine or areas where heat conduction and convection take place. Sun et al. [17] numerically investigated the behaviour of corrugated truss cores using models with industrially useful dimensions; however, the simulations results were not validated using any experimental data. It is pertinent to mention that Tonlli et al. [18] provided a critical evaluation of the sandwich beams mechanics using numerical models that are realistic and can replace previous studies that may be limited to a certain range of beams' stiffness or do not count for all the physics associated to the beams' mechanical behaviour.

Recently, more attention [19-21] has been paid to permeable/cellular continuous surface structures such as triply periodic minimal surface architectures due to their enhanced strength and stiffness combined with reduced density. Some investigations utilised [22-25] various filling materials to increase the structures' stiffness and their impact absorption tolerance. Since 3D printing is a suitable method for manufacturing such structures, Qin et al. [21] characterised 3D printed graphene gyroid material in terms of its tensile and compressive strength. Although various cell sizes and material densities were investigated, only tube-shaped samples were created and they were not compared to any other readily available structures such as auxetic, honeycomb or lattice truss structures. The use of triply periodic minimal surface architectures in the sandwich beams application may have a great potential to serve the research of interest in this paper.

From the literature, it can be noted that the research in this area is in its infancy so far and a full understanding of the behaviour of the 3D printed cores is still required. In a previous work [26], we conducted a numerical and experimental study on 3D printed honeycomb and auxetic structures and compared their strength to the commercially available aluminium honeycomb cores. Although the Al cores offered the highest normalised strength and stiffness, the re-entrant cores were superior in terms of both flexural strength and stiffness, which can be significantly important in strength-critical applications. Despite that, only one unit-cell size was utilised for each core design and an intensive study is still needed to investigate a wider range of core designs. In this paper, bending strength and stiffness of seven different core structures were investigated for motorsport and aerospace applications including, for the first time, triply periodic minimal surface structures which were not used before in the composite sandwich materials. Industrial relevance is achieved using relatively large-scale samples with CFRP face sheets as commonly used in the industry.

2. Material and Experimental Setup

Seven different cores were designed and fabricated including Honeycomb with small (HS) and large (HL) cell sizes (Fig 1), Re-entrant honeycomb from the class of auxetic core structures with small (RS) and large (RL) cell sizes (Fig 2), Pyramid (P) and Hierarchical Pyramid (HP) lattices from the octahedral core class (Fig 3-4) and lastly a triply periodic minimal surfaces (TPMS) structure known as Gyroid (G) [27] (Fig 5).

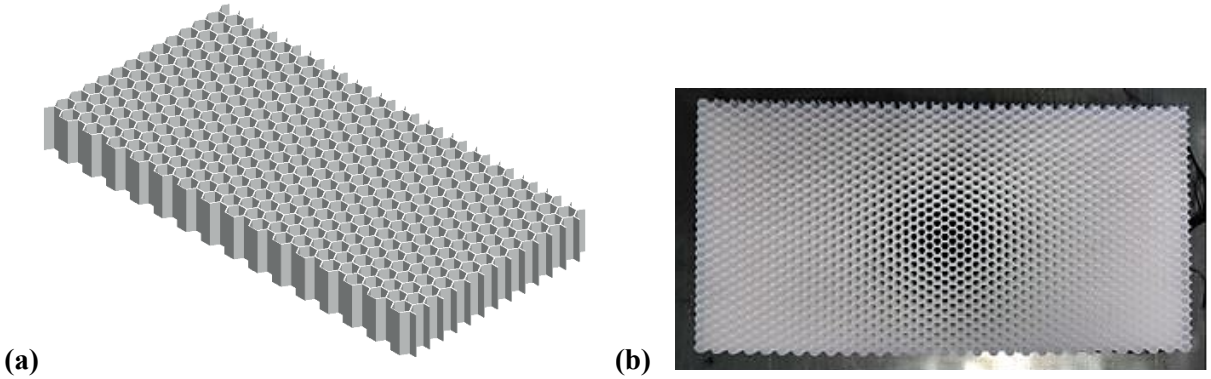

Fig 1. (a) A CAD model of the Honeycomb core structures **(b)** 3D printed sample.

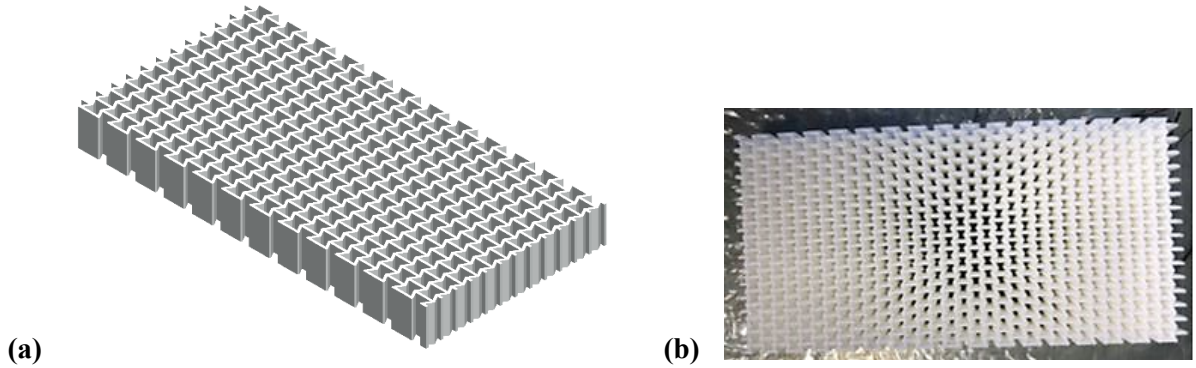

Fig 2. (a) A CAD model of the Re-entrant honeycomb core structures **(b)** 3D printed sample.

The two pyramid lattice structures shape shown in Fig 3 and 4 were created based on the structures numerically investigated in [17] and the cores' dimensions provided in the appendix were selected based on the manufacturing constraints as well as avoiding undesired buckling of the struts, which may cause premature failure.

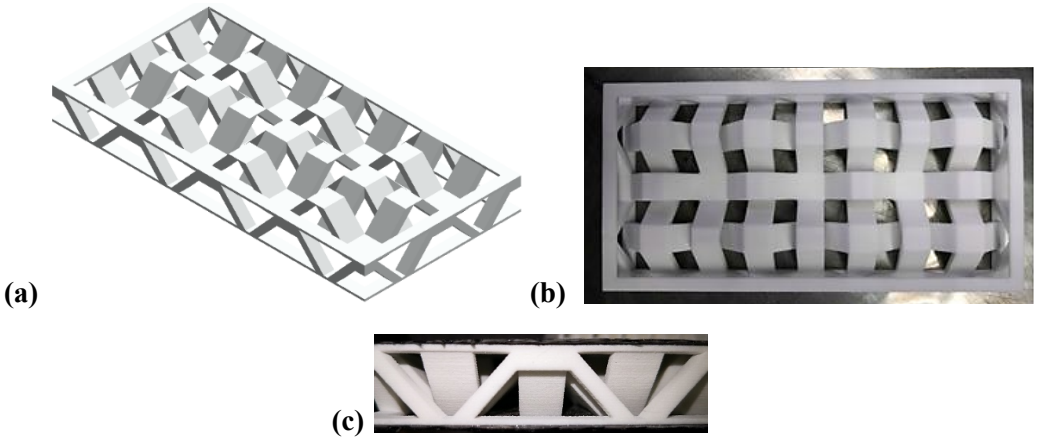

Fig 3. (a) A CAD model of the pyramid lattice structures **(b)** 3D printed sample **(c)** A side view showing the struts

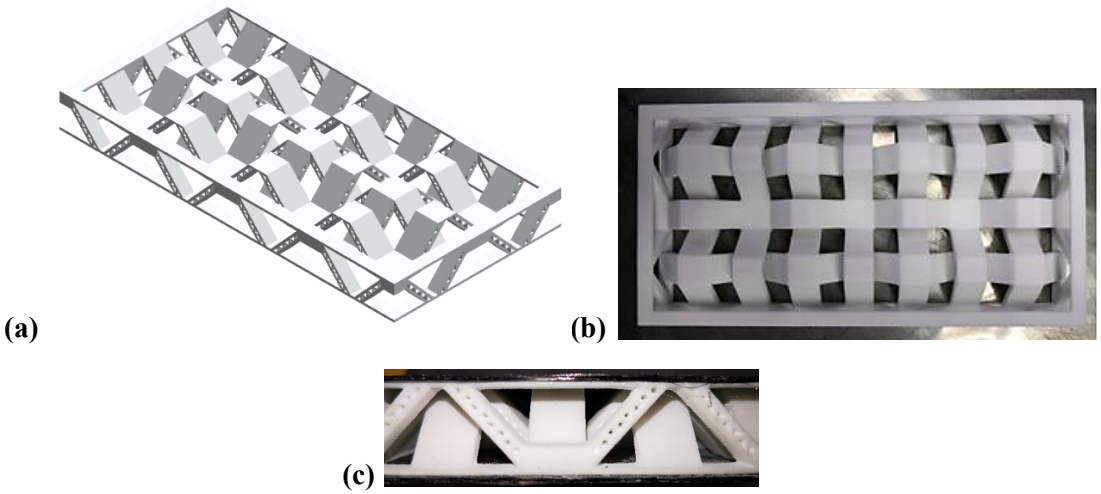

Fig 4. (a) A CAD model of the hierarchical pyramid lattice structures **(b)** 3D printed sample **(c)** A side view showing the hierarchical struts

For the structures, the gyroid's wall thickness was kept at 1 mm, consistently with the other cores' dimensions. For more details on this core's design, please refer to the appendix.
The unit cell curve of the gyroid structure shown in Fig 5 can be expressed using the following formula [28]:

$$f(x, y, z) = a\,(\sin x \cos x) + b\,(\sin x \cos z) + c\,(\sin z \cos y) + \beta \quad (1)$$

Where a, b, and c are spatial variables that range over an interval of 2π to generate a unit cell, while β is used to determine the required solid fraction. The "strut angle" term is also used to identify the angle between the internal beams (struts) that transmit the loads within the cores' structures, for more information please refer to [29]. Variables a, b, and c are also used to control the shape of the TPMS unit cell when certain strut angle is used to support internal loads in a certain direction or when manufacturing parameters determine the boundaries of the cell's dimensions. The strut angle used in this research is 45º to ensure isotropic mechanical properties and a homogeneous distribution of mass across the core. Previous research [29] studied the gyroid's compressive strength and proposed a preferred deformed unit cell shape using the principle of the strut angle to provide the required strength in the uniaxial direction. Due to the nature of the application investigated in this article, three-dimensional shear and normal stresses will develop in the core and hence the structural unit cell needs to support the loads in all direction, hence the gyroid geometry, detailed in the appendix, was selected for this work.

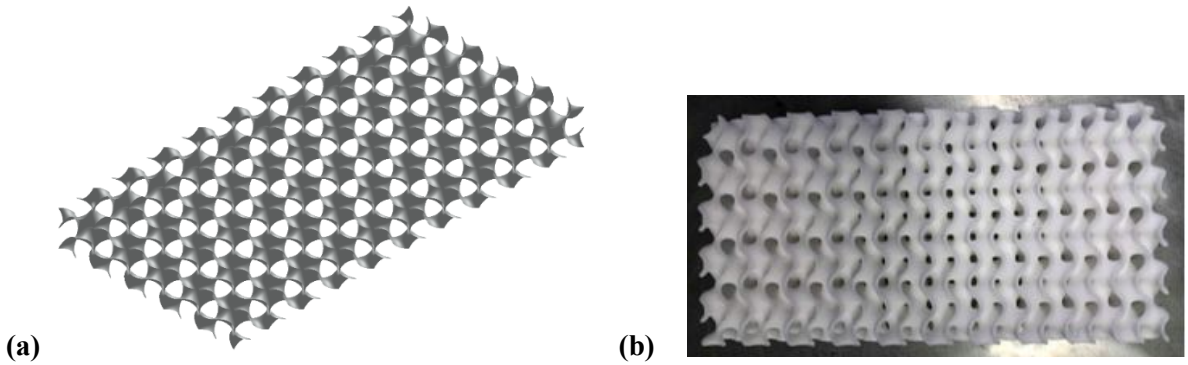

Fig 5. (a) A CAD model of a triply periodic minimal surfaces structure (Gyroid) core structures **(b)** 3D printed sample.

The face composite sheets shown in Fig 6 were fabricated using carbon fibre 2/2 twill weave 3k 240 g sheets. A wet layup technique with each skin made up the three sheets using a quasi-isotropic layup method, EL2 Epoxy Laminating Resin mixed with AT30 slow epoxy hardener at a ratio of 100:30 which was used to give a final sheet thickness of 1

mm. The samples were cold cured at room temperature over 24 hours to prevent any potential degradation of the 3D printed cores properties that usually occur with accelerated curing processes such as the use of an oven. The sheets were attached to the cores using the same type of epoxy.

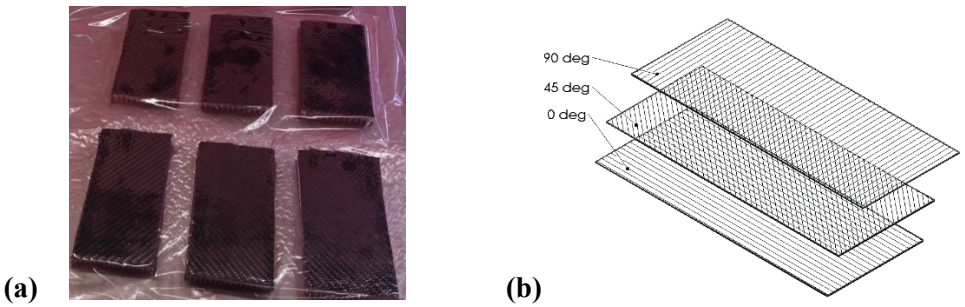

Fig 6. (a) A face composite sheet using carbon fibre 2/2 twill weave 3k 240g **(b)** the layers lay-up angles

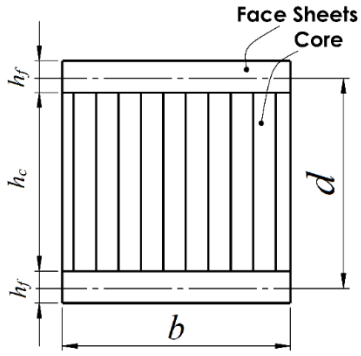

Fig 7. Basic dimensions of the sandwich beams.

Carlsson and Kardomateas [30] provided a practical condition Eq.3 that can be used to determine whether the face sheets are considered thin. If the ratio is less than 5.35, the face sheets are considered thick and the beam will perform as a stiff component and may not fully utilise the combination of the flexible but weak core when it is combined with the strong and stiff face sheets.

$$\frac{h_c}{h_f} \geq 5.35 \tag{3}$$

This condition is satisfied in our case with a thickness ratio of 13/1 which ensures a balanced CFRP skins behaviour. Thicker skins may not meet the aforementioned requirement due to increasing the beam's weight, providing excessive stiffness and significantly reducing the core's contribution to the sandwich functionality. Moreover, a reasonable thickness of 1 mm will eliminate the likelihood of the beam's failure due to localised compression and skin wrinkling that result from using excessively flexible skins that are usually weak under compression. Table 1 gives the values of the mass density of all the designed cores.

Table 1. Process parameters and Nylon PA2200 material properties

Core Type	Honeycomb large (HL)	Honeycomb small (HS)	Re-entrant Large (RL)	Re-entrant Large (RS)	Pyramid (P)	Hierarchical Pyramid (HP)	Gyroid (G)
Mass density [g/cm3]	0.327	0.381	0.535	0.561	0.414	0.383	0.486

All of the cores were 3D printed using EOS PA2200 powder (also known as Nylon PA12) which was laser fused using a FORMIGA P110 machine. The parameters for the process are given in Table 2. The overall sample dimensions are 150×75×17 mm³. The three-point bending test was carried out using a Testometric FS500CT 500 kN machine with a 20 mm/min (0.33 mm/s) loading speed, 20 N preload, a span of 110 mm and a maximum deflection limit of 25 mm to ensure a safe deformation of the samples without losing contact with the supporting pins. The loading and supporting pins diameters were 30 mm and 10 mm respectively (see Fig 8).

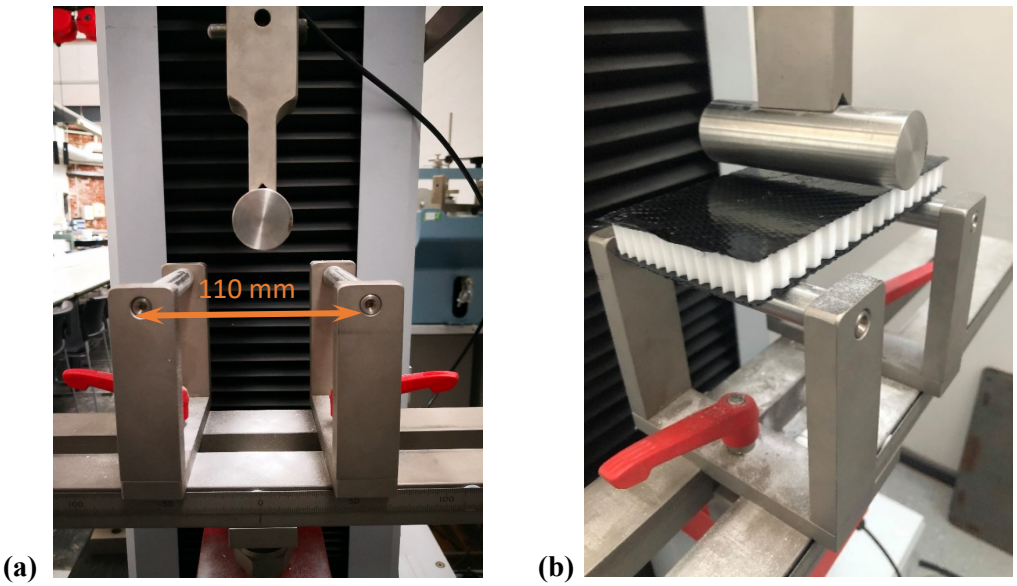

Fig 8. Three-point bending test setup **(a)** span distance **(b)** loading pin position on the sample

Table 2. Process parameters and Nylon PA2200 material properties [31, 32]

Process Parameters		**Material's Properties**	
Laser Type	CO2, 10.6 µm	Bulk Density [g/cm^3]	0.45
Laser Power [W]	30	Laser-Sintered Part's Density [g/cm^3]	0.93
Scanning Speed [m/s]	5	Ave. Particle Size [µm]	56
Layer Height [mm]	0.1	Tensile Modulus [MPa]	1700
Scanning Direction	Y	Tensile Strength [MPa]	48
Processing Temp [ºC]	170	Melting Temperature [ºC]	172-180

3. Results and Discussion

-Failure and delamination

All samples were tested using the three-point bending test to evaluate the flexural strength, modulus and stiffness. Except for the gyroid and the pyramidal structures, all sandwiches shown in Fig 9 suffered from deformation and failure at the centre of the core due to a crack initiated in the lower part where the maximum bending tensile stress is accompanied with shear stress. The two pyramidal structure failed to the left of the loading pin while the gyroid structure withstood the load without breakage and only showed plastic deformation until the loading pin exceeded the pre-determined 20 mm displacement. For both pyramidal samples, a localised fracture is observed at the edge of the sample which did not propagate through the entire structure as observed in the other cases.

Generally speaking, the core structures ultimately fails due to in-plane shear stresses developed in the core, induced by the shear forces at the middle of the span; however, more details will follow in the next subsection to discuss the failure mechanism of each core type. It is important to note that the exact failure location due to in-plane shear stresses may not always be located at the centre of the sandwich due to many reasons including manufacturing defects such

as un-sintered powder particles, porosity and the weak connection between the 3D printed layers etc. Under excessive stresses, such imperfections act as nuclei for cracks initiation and propagation within the cores until the material's maximum distortion energy is exceeded and failure occurs. Depending on the application to be served by the sandwich beam, an intensive design optimisation study is needed for each core to optimise the cores dimensions, weight and cost, but this type of studies is beyond this article's scope.

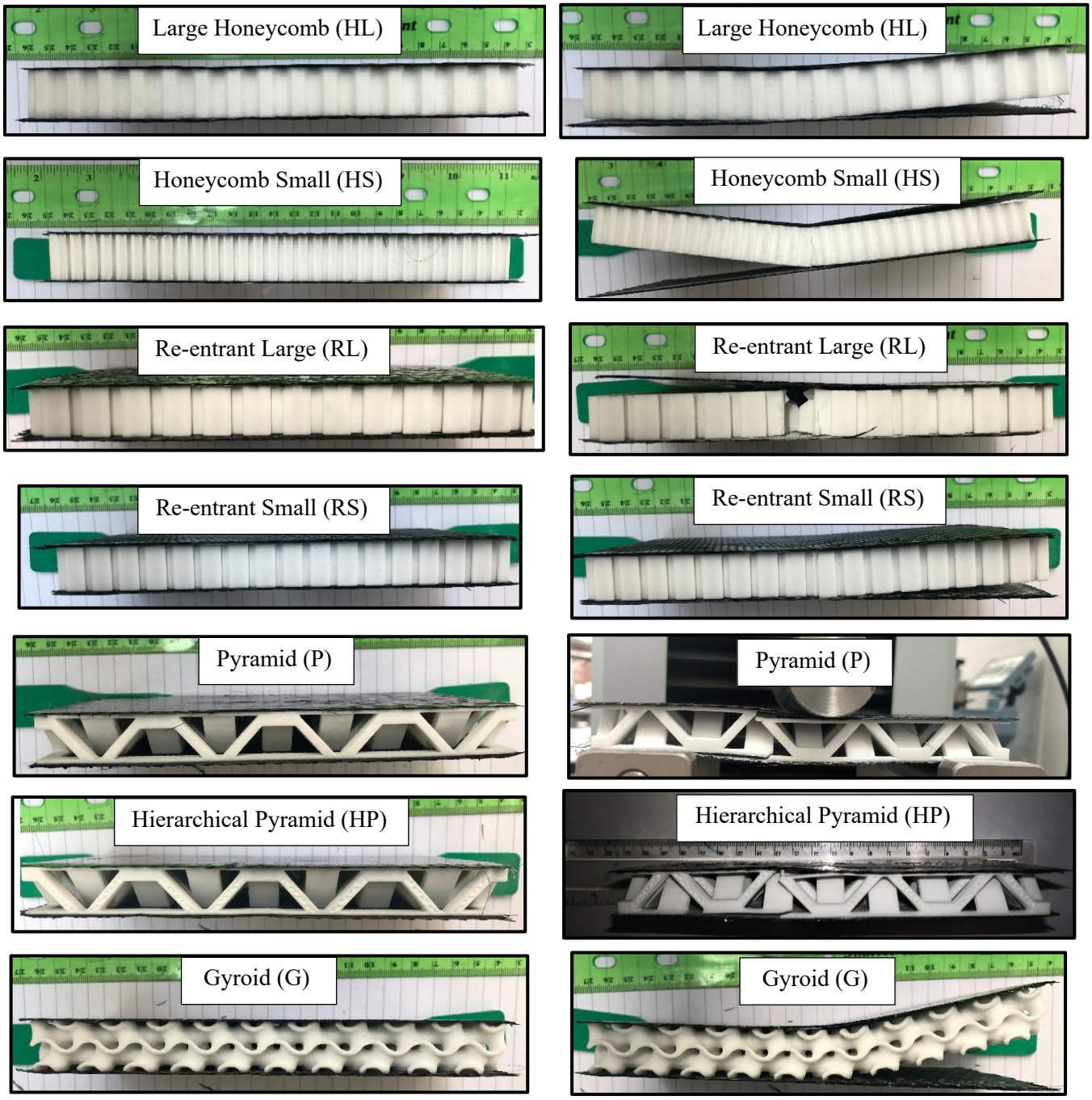

Fig 9. Composite sandwiches prepared for testing (left) and the deformed sandwich beams after the three points bending test (right)

All sandwiches suffered from face/core debonding at either the bottom or the top adhesive layer, or both as in HS (see Fig 9). Due to the composition of the core's material, it is not possible to fabricate an integral and co-cured sandwich structure that offers a very strong adhesion between the sandwich components. Due to the use of the manual layup of the large preformed composite sheets, the adhesion of the two components may vary over the large area and the face/core interface may include invisible and small areas of poor bonding that may be represented by "islands"

or small cracks. Using the linear elastic fracture mechanics concepts and according to Hutchinson and Suo [33], those interface cracks between two different materials are inherently loaded in mixed-mode stresses because of the contrast in the materials physio-mechanical properties across the crack interface. Therefore, although the in-plane shear stresses are usually minimal at the core/face interface, the complex state of stress at the crack's tip aided with the tensile and compressive normal stresses at the sandwich bottom and top respective sections lead to the separation shown in Fig 9. Due to the complexity of the delamination mechanism that significantly depends on the morphology of the adhesive layer, it is difficult to predict the location of the debonding but it is easier to observe when it happens by analysing the force-displacement or stress-strain diagrams of the sandwiches. Although a stronger adhesion can be achieved by thermal curing of the adhesive in an oven or using UV light, both processes are not recommended for the 3D printed components to avoid any degradation of PA12 properties and deviation in the bending results [31]. This justifies the use of the EL2 Epoxy adhesive which is cold-cured and does not impose any potential change to the 3D printed material's properties.

In addition to the previous analysis related to the face sheet morphology, other factors may contribute to the face/core interface debonding. Honeycomb cores show a well-known anticlastic behaviour which induces a secondary curvature at each end of the sandwich core when it is under bending. The behaviour is more pronounced away from the core's centre and may contribute to the skins' delamination on both sides. The Re-entrant structures show a synclastic effect characterised by a negative Poisson ratio causing a secondary curvature in the opposite direction to that seen in the honeycomb structures, forming a dome-like shape under bending [34]. This variable curvature induces in-plane shear and normal stresses at the skin-core interface aiding the separation observed in Fig 9.

This syn- and anti-clastic behaviour does not exist in other structural cores such as the pyramidal and the gyroid. However, fabrication defects and the islands of weak adhesion may cause skin separation when the sandwich structure experience large displacements. It should be noted that no delamination took place in the pyramidal structures during the test until the core failed and caused a localised separation of the skin. This may be attributed to the top and bottom supporting frames needed for holding the pyramidal cells together, which do not exist in other cores. Those frames are design-essential features in the pyramidal cores but not necessary for other cores and they increase the sandwiches weight.

3.1 Strength and Stiffness

Presented in Fig 10 and 11 are the relationships of the force against displacement and stresses against strains respectively. Both figures contained subgraphs (a) and (b) to avoid data overlapping and to ensure clarity. Form those figures, a distinct behaviour can be observed for various core structures in terms of the maximum flexural load, plastic and elastic strains and sometimes the absence of significant plastic deformation. The force-displacement curves shown in Fig 10 and 11 start with a linear relationship (elastic region) that ends with a sudden drop in the force value, indicating a skin delamination and noted by a single cracking sound during the test. The force afterwards resumes its climbing until the core's damage takes place at different displacement values for various structures. The curves for some structures such as HL and HS exhibited multiple significant drops corresponding to a skin delamination at different locations in the beam structure, while other curves (P and HP) did not indicate any delamination before their ultimate failure.

It is also important to note that core structures behaved in a ductile fashion until failure evidenced by the large plastic deformation quantified in Fig 10 and 11 with a maximum value of displacement of 25 mm. The small re-entrant core structure supported the largest maximum load of 2119 N, followed by the gyroid and large re-entrant cores which supported about 2070 N and 2022 N respectively. Both honeycomb structures showed the weakest performance by supporting the least maximum load in the range of 441-447 N, while the hierarchical pyramid lattice structures showed a moderate performance.

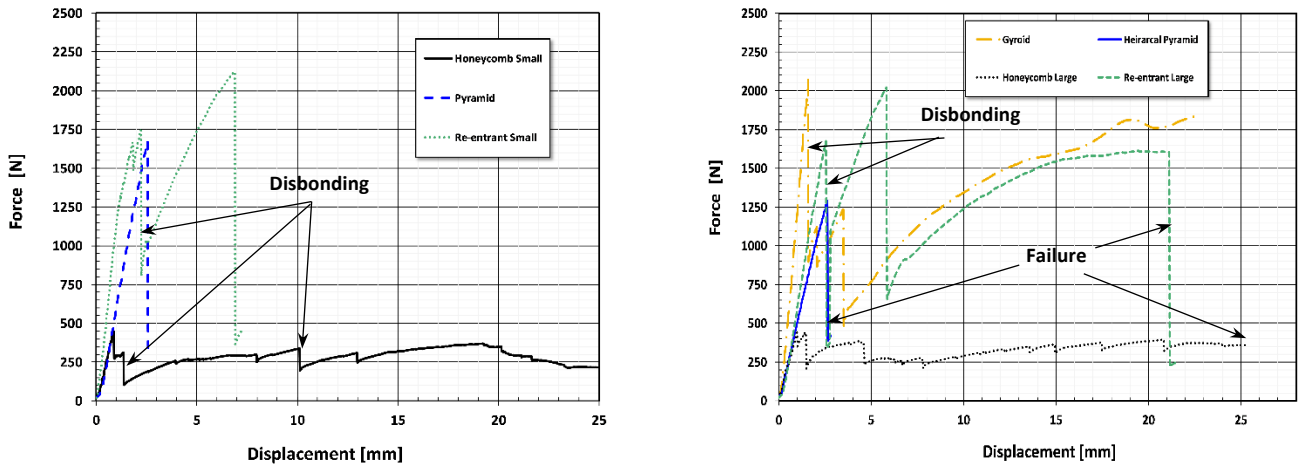

(a) **(b)**

Fig 10 Loading force in Newtons against displacement for **(a)** HL, RL, HP and G and **(b)** HS, RS and P cores.

A similar trend can be seen in the stress-strain diagrams, as shown in Fig 11a and b, in which the maximum flexural strength was recorded in the case of the small re-entrant structures with a value of 8.8 MPa although the ultimate strain was about 30% of that of the large re-entrant. The small re-entrant ultimate strength value is not distant from the gyroid sandwich strength of about 8.6 MPa, at about 1.3% strain, with the second-highest flexural modulus after that of the large re-entrant cores.

Although the honeycombs cores achieved the least flexural strength (1.8 MPa at 1.6% strain) among all cores, they are the only cores which achieved the largest deflection of about 25.5 mm (17.8% strain at failure) followed by the gyroid core with a deflection of 22.8 mm (16% strain). All the rest cores, except the large re-entrant, showed a relatively low strain of less than 7% before failure took place. It is pertinent to mention that the recorded flexural forces significantly fluctuated against deflection for all cores except for the honeycomb cores whose forces changed in a small range of about 300 N.

The large drops seen in the force curves can be related to the debonding of the skins and degradation of the sandwich structure integrity. At that point, the core started to carry a larger portion of the load and the force gradually rose with the plastic deformation of the cores' cells until failure takes place. Since the debonding did not occur in the P and HP cores, the force and stress curves only show one peak representing the cores' failure.

The "telegraph-signal" shape detected in some of the curves in Fig 10 and 11 may indicate individual fibres failure in the composite sheets which is a well-known behaviour in composite materials failure [35]. The use of carbon fibre sheets with a larger number of fibres in the single tow (6k, 12k sheets) may increase the strength of the skin composite and could further enhance the performance of the sandwich composites; however, this would have a negative impact on the sandwiches' weight.

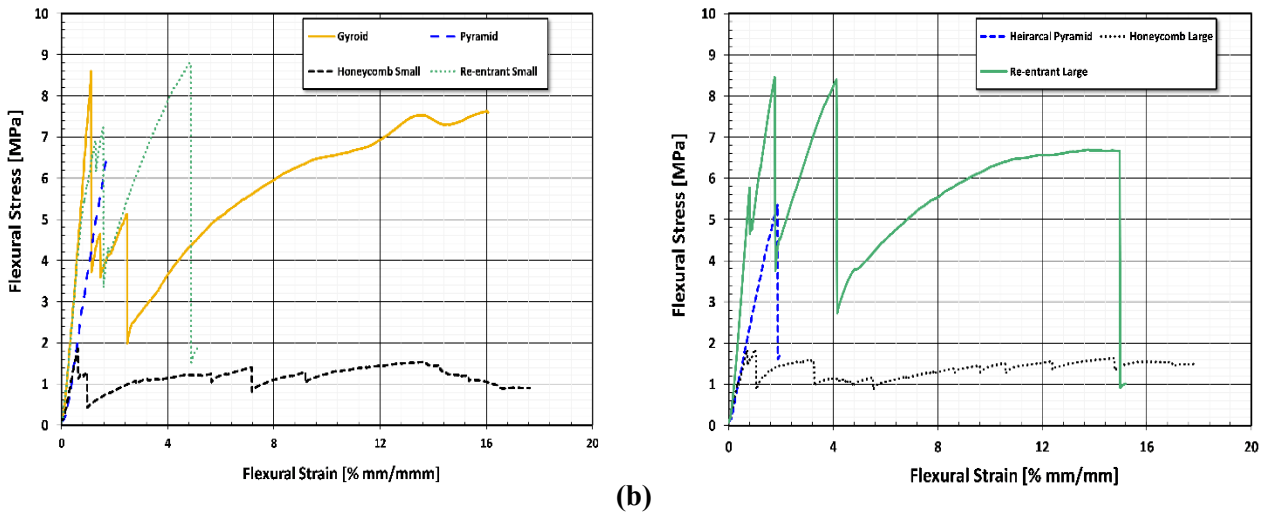

(a) **(b)**

Fig 11. Flexural stress and strains for **(a)** HL, RL, HP and G and **(b)** HS, RS and P cores

Fig 12 provides a quantitative comparison of the ultimate strength and the flexural modulus among all tested beams. It is evident that the re-entrant cores were significantly stronger than the honeycomb HS and HL by about 4.5 times and had a larger modulus by about 2.5 times. This significant difference between those two types was consistent with the results found by Harland et al. [26] who indicated a superiority of the re-entrant cores over conventional Aluminium and 3D printed honeycomb cores due to the auxetic behaviour that promotes increased resistance to deformation under bending loads.

It is pertinent to mention that the use of a reasonable functional sample size such as the one used in this investigation makes the deformation and failure mechanism more complicated with the negative Poisson ratio effect due to the transverse collapse of the beam's upper half under compressive stresses, while the bottom half, on the contrary, tend to transversally expand under the tensile bending stresses. Additionally, a mixture of both behaviours will be experienced in other regions in the core structures.

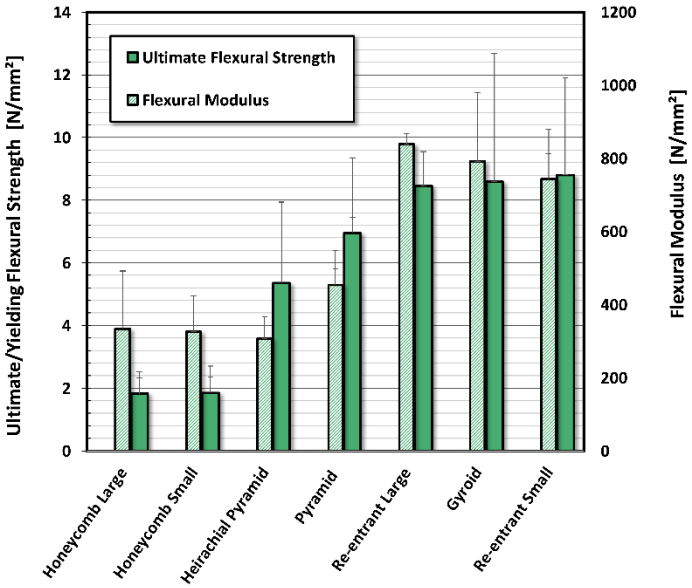

Fig 12 The flexural ultimate strength and modulus obtained from the three-point bending test

It can be proved from Fig 12 that the hierarchal structure reduced the strength of the pyramid core by about a third and both structures did not show any significant plastic deformation. This may be related to the presence of the thin frame holding the core's cells together, which was the weakest point and did not allow for an effective transfer of the force to the core. Making this feature as thin as possible is essential for reducing the core's thickness h_c and for

avoiding any direct contribution to the cores' stiffness that should be mainly supported by the composite face sheets as in all other sandwich beams. From our results, it is recommended that pyramid structures should only be used with a 3D printed skins of the same material to ensure the consistency in the support of the face sheets, or when thicker core frames are permitted.

Finally, the gyroid (G) structures were very close in their behaviour to the RL by withstanding a very similar force and deflection, but without a fracture in the core. The gyroid surface continuous and smooth curvature within the core may have significantly promoted smooth load transfer and reduced stress concertation that can easily be spotted in other cores structures that include sharp nodes in their design [28]. This can also be the reason behind the resistance to fracture at high strain values and the ability to gradually adjust the cells' shape, making the structure more damage tolerant and stiffer than other cores. Another advantage of the gyroid structure is its periodicity in three-dimensional directions compared to other structures which do not offer isotropic properties and may develop discontinuous strain field that, combined with the stress concentration, promote failure at the sharp nodes. From this initial observation, a clear advantage of the gyroid cores can be seen.

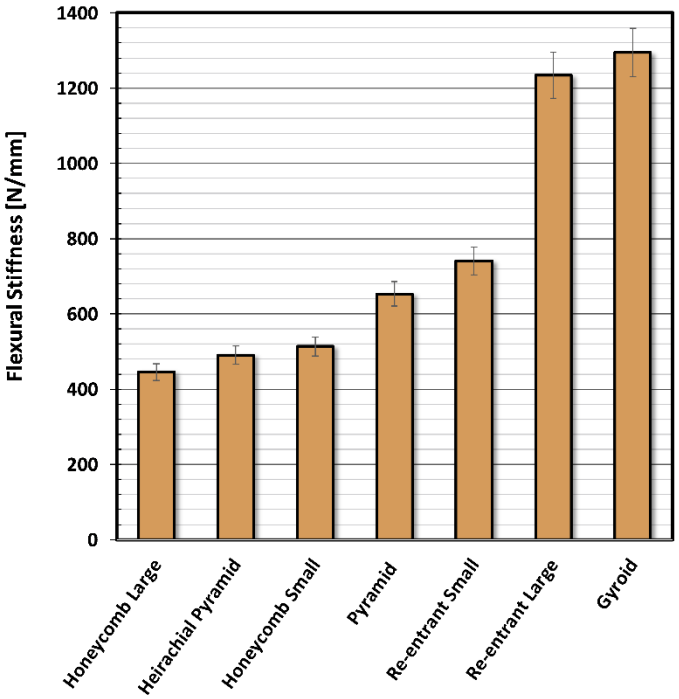

Fig 13 The flexural stiffness [N/mm] calculated as the ratio of the maximum bending load and its corresponding displacement

According to Fig 13, gyroid cores achieved the maximum stiffness value of about 1310 N/mm while honeycomb cores and pyramid cores were located in the low-values range. Although the RS core achieved a higher strength than the gyroid by about 3.5%, its stiffness was less than the gyroid by about 4.6%.

It should be noted that the RL structure showed more flexibility and hence more deformation tolerance than the stronger RS structure due to the larger volume fraction (spaces between the cells) that allowed for more efficient utilisation of the negative Poisson ratio effect compared to RS cells. Larger volume fraction means that the cells have larger inner space to collapse and expand under loading and hence absorb more energy than stronger structures with less volume fraction. Therefore, it can be said that the stiffness and the modulus of the RL are significantly larger than those of the RS although the latter resisted a larger bending force.

Given that the areas located under the G and RL stress-strain curves are the largest, those structures are considered the toughest and the most damage-tolerant evidenced by the largest stiffness value among all other structures. Between those two structures, the gyroid core did not exhibit a fracture failure and recorded the largest stiffness value

of 1310 N/mm; therefore, it can be said that the gyroid core is the best performing structure of all tested sandwiches when both stiffness and strength are considered.

3.2 Normalised Strength and stiffness

To be able to compare the different cores' performance and their ability to support weight-critical applications, the values of strength and stiffness were normalised using the sample weights in Newtons as shown in Fig 14. This figure shows that the gyroid core structure provided the highest normalised flexural strength, modulus and stiffness of all the sandwich samples tested.

The pyramid (P) and the RL structures provided the second-highest normalised strength and stiffness respectively, pushing the RS, which was the strongest, to the relatively low-values range. Consistent with their position in the strength and stiffness values, the honeycomb cores did not offer a significant normalised strength and stiffness values.

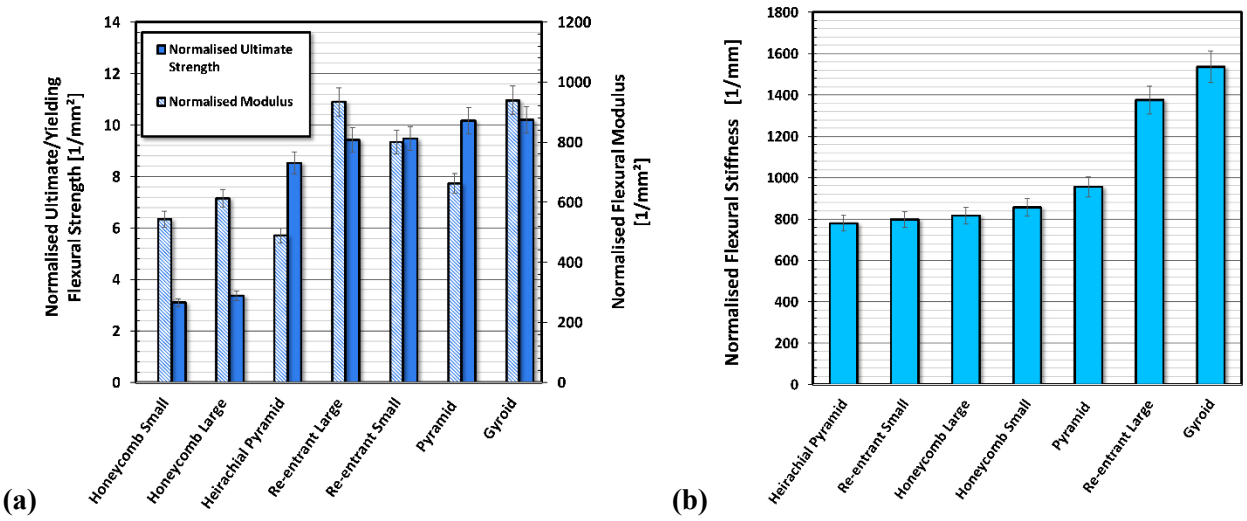

Fig 14 The normalised/specific **(a)** flexural ultimate strength and modulus **(b)** flexural stiffness

It is pertinent to mention that the weight of Nylon PA12 cores evaluated in this investigation not only can be adapted by changing their cells' size and shape and the cores' overall dimensions, but it can also be significantly reduced by adopting a variable resolution across the core that can be coarse towards the edges and fine at the core's centre where the minimum and maximum loads and stresses are respectively located. Design considerations such as the requirement for assembly hardpoints or fixing holes can also be satisfied and incorporated into the core's design, eliminating the need for post-machining and its associated defects that may act as stress raisers.

4. Conclusions

In this article, the strength and stiffness of various novel 3D printed core structures were investigated and compared to conventional structures. 3D printing offer a tool to create core stuctures of acomplex shapes that cannot be manufactured From this work the following conclusions can be drawn:

1. The small re-entrant sandwich supported the largest load of about 2120 N among all tested cores.
2. Despite withstanding large strain values, the honeycomb cores were the poorest in terms of the flexural ultimate strength and stiffness.
3. The large Re-entrant and the gyroid sandwiches were the toughest among all tested cores.
4. The gyroid core structure showed the highest damage tolerance characteristics without fracture, even after a deflection of 25 mm.
5. The gyroid core structure achieved the highest strength and stiffness to weight ratio which is vital in all weight-critical applications such as motorsport and aerospace.

Appendix

In this appendix, detailed dimensions of the unit cells for each core structure are provided. In Fig A-1 and A-2, the dimensions of both the large and small sized honeycomb and re-entrant structures are respectively provided along with a 3D isometric view.

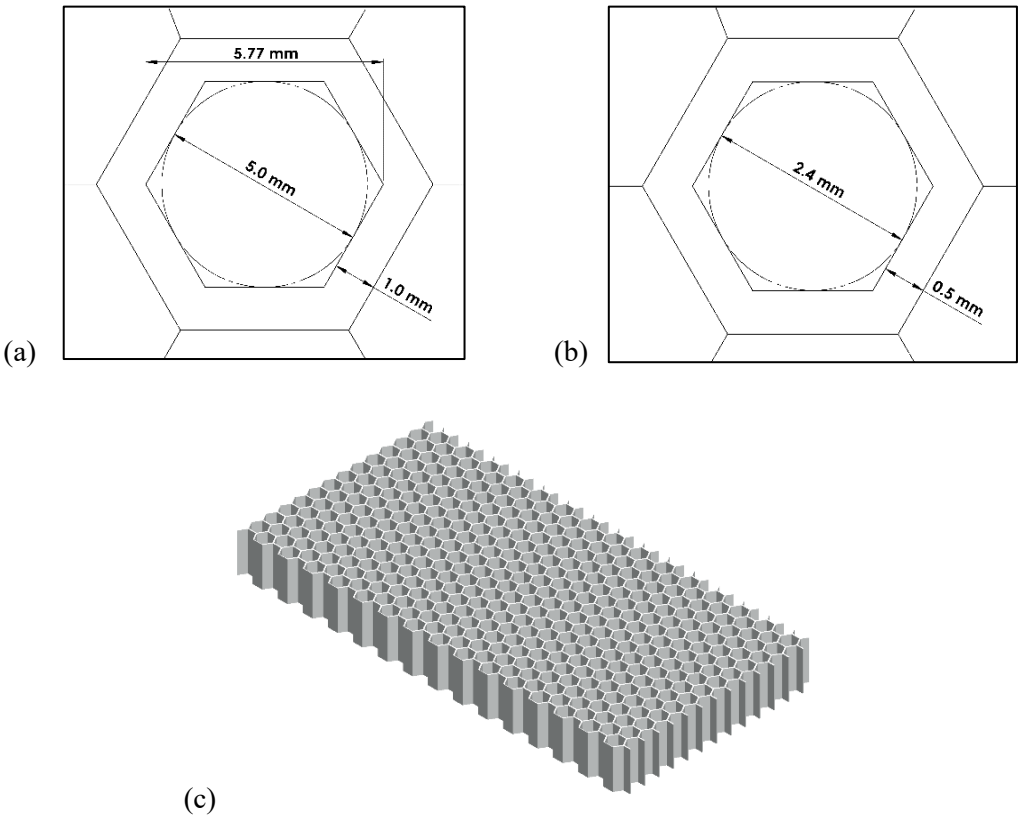

Fig A-1 Dimensions of the **(a)** large and **(b)** small honeycomb structures unit cell **(c)** a three-dimensional CAD model

The re-entrant structures are well known for their negative Possion ratio which gives them a competent resistance to compression and the ability to withstand large deformation before failure. Those structures along with the honeycomb hexcells were selected as a benchmark due to their ever use in sandwich panels fabrication [26].

In Fig A-3, the gyroid unit cell's diemnsions are given with some auxialliary arc radii are provided to asssit repeatability. The gyroid structure were selected due to their tripley periodicity and their minimal surface that are usually found in nature due to homogeneous tension. This mean that those structures provides the minimum density in a given periodicity and hence provides the sandwich beams with the minimum density for a given cores' volume [21]. In addition, the ease to scalability and their high resistance to compression make them a potential structure to examine in the sandwich beams' loading environment [36].

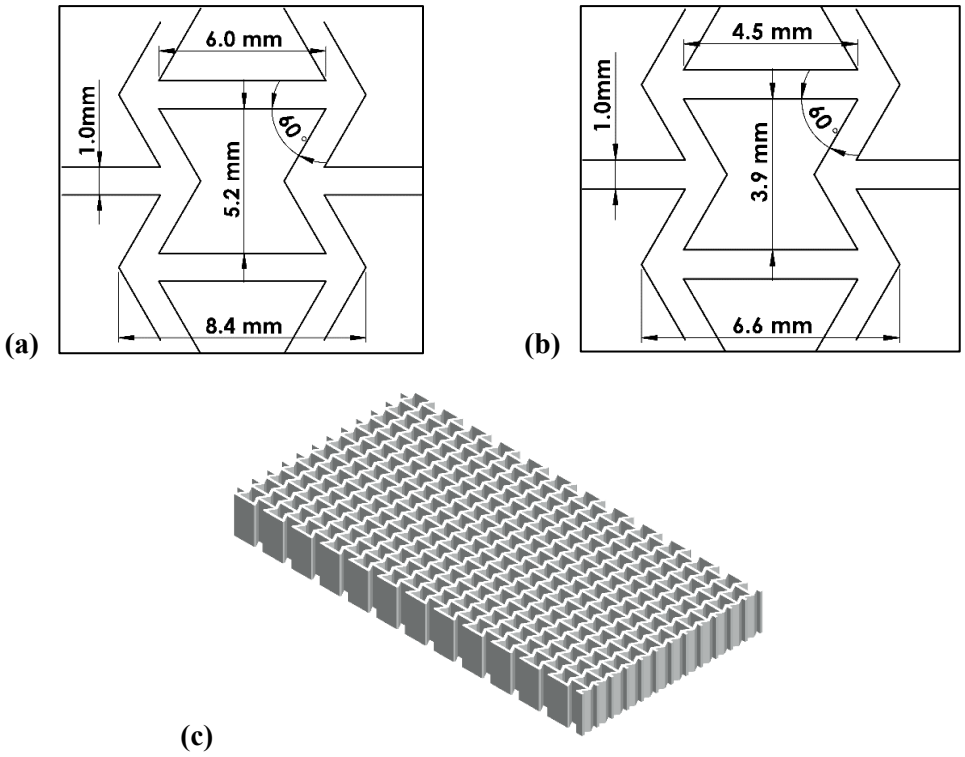

Fig A-2 Dimensions of the **(a)** large and **(b)** small re-entrant structures unit cell **(c)** a three-dimensional CAD model

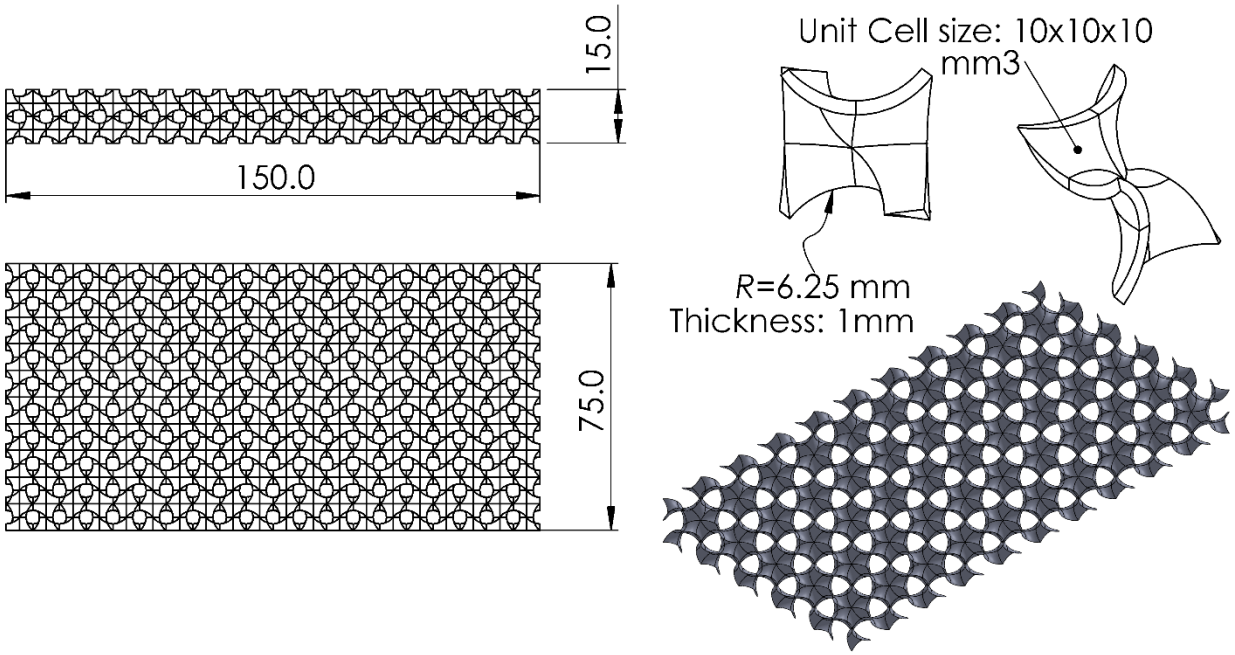

Fig A-3 Dimensions of the gyroid core structures

The pyramids depicted in Fig A-4 and A-5 were constructed using a strut (supporting bar) angle of 47.5º separated by 10 mm distance and an overall thickness of 15 mm, consistently with the other sandwiches' thickness. When adding a hierarchy, a corrugated structure was placed at 2 mm intervals to investigate their effect on the cores' behaviour.

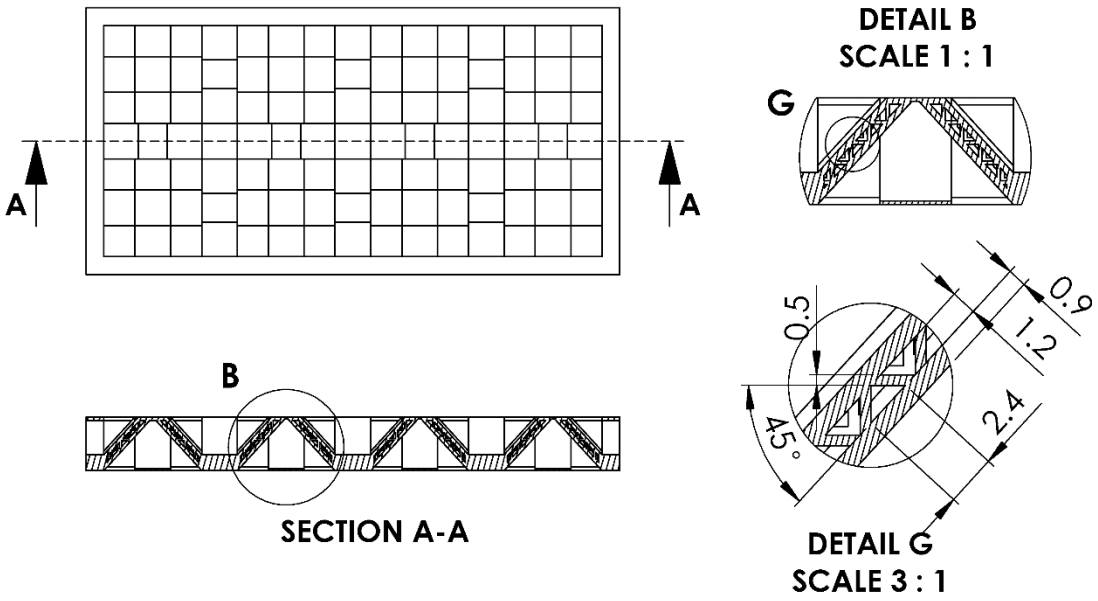

Fig A-4 Dimensions of the pyramid core structures

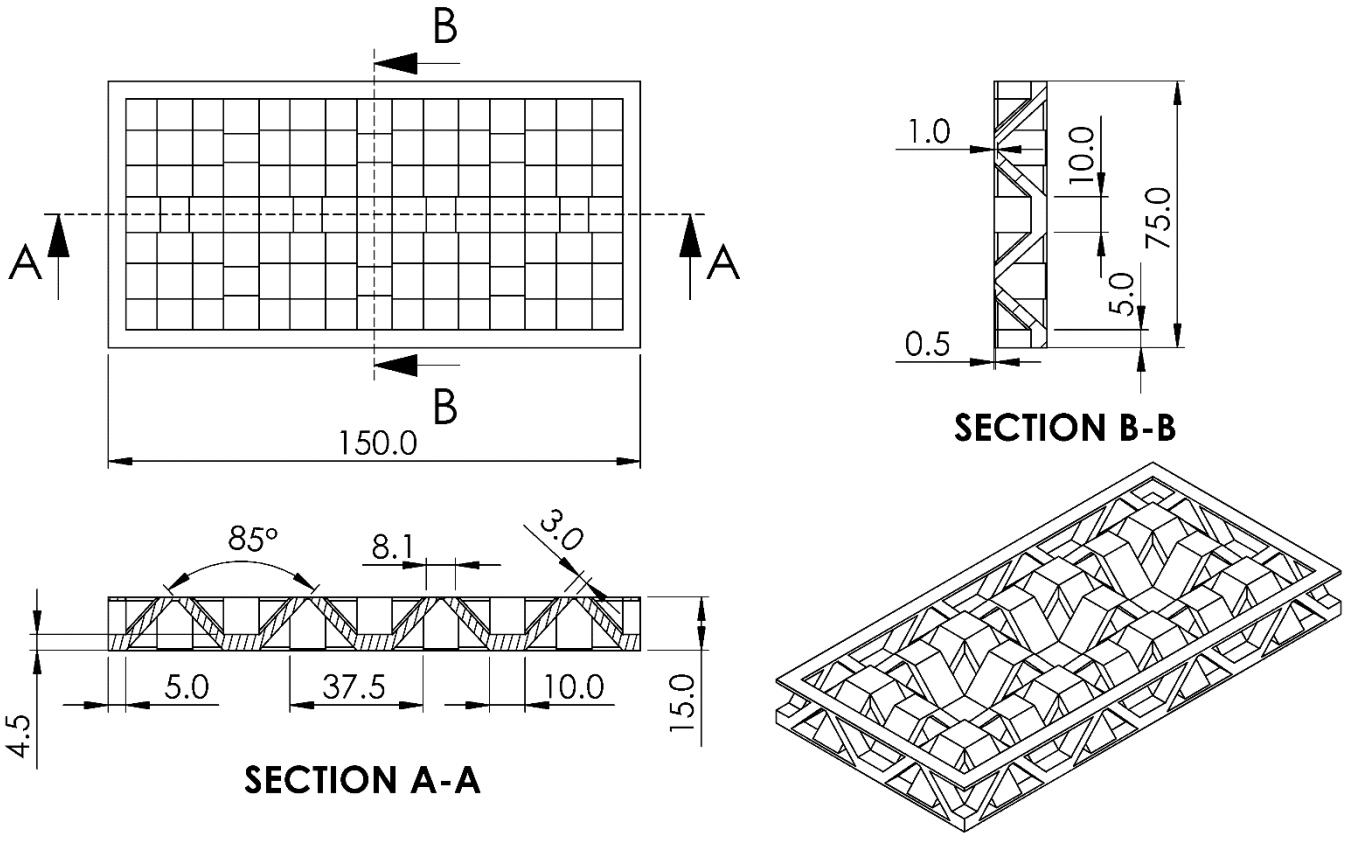

Fig A-5 Dimensions of the hierarchal pyramid core structures

5. References

1. Schaedler TA, Carter WB. **Architected Cellular Materials**. Annual Review of Materials Research;46(1)(2016):187-210.
2. Ashby M. Metal foams: a design guide: Boston: Butterworth-Heinemann; 2000.
3. Burton WS, Noor AK. **Assessment of continuum models for sandwich panel honeycomb cores**. Computer Methods in Applied Mechanics and Engineering;145(3)(1997):341-60.
4. Rathbun HJ, Radford DD, Xue Z, He MY, Yang J, Deshpande V, et al. **Performance of metallic honeycomb-core sandwich beams under shock loading**. International Journal of Solids and Structures;43(6)(2006):1746-63.
5. Petras A, Sutcliffe MPF. **Failure mode maps for honeycomb sandwich panels**. Composite Structures;44(4)(1999):237-52.
6. Buitrago BL, Santiuste C, Sánchez-Sáez S, Barbero E, Navarro C. **Modelling of composite sandwich structures with honeycomb core subjected to high-velocity impact**. Composite Structures;92(9)(2010):2090-6.
7. Rodriguez-Ramirez JdD, Castanie B, Bouvet C. **Experimental and numerical analysis of the shear nonlinear behaviour of Nomex honeycomb core: Application to insert sizing**. Composite Structures;193(2018):121-39.
8. ALLEN HG. Analysis and Design of Structural Sandwich Panels, A volume in The Commonwealth and International Library: Structures and Solid Body Mechanics Division: Elsevier Ltd; 1969.
9. Martin JJ, Fiore BE, Erb RM. **Designing bioinspired composite reinforcement architectures via 3D magnetic printing**. Nature Communications;6(1)(2015):8641.
10. Zhang Q, Zhang F, Medarametla SP, Li H, Zhou C, Lin D. **3D Printing of Graphene Aerogels**. Small;12(13)(2016):1702-8.
11. Hou Z, Tian X, Zhang J, Li D. **3D printed continuous fibre reinforced composite corrugated structure**. Composite Structures;184(2018):1005-10.
12. Dikshit V, Yap YL, Goh GD, Yang H, Lim JC, Qi X, et al. **Investigation of out of plane compressive strength of 3D printed sandwich composites**. IOP Conference Series: Materials Science and Engineering;139(2016):012017.
13. Yazdani Sarvestani H, Akbarzadeh AH, Niknam H, Hermenean K. **3D printed architected polymeric sandwich panels: Energy absorption and structural performance**. Composite Structures;200(2018):886-909.
14. Wu Q, Gao Y, Wei X, Mousanezhad D, Ma L, Vaziri A, et al. **Mechanical properties and failure mechanisms of sandwich panels with ultra-lightweight three-dimensional hierarchical lattice cores**. International Journal of Solids and Structures;132-133(2018):171-87.
15. Li T, Chen Y, Hu X, Li Y, Wang L. **Exploiting negative Poisson's ratio to design 3D-printed composites with enhanced mechanical properties**. Materials & Design;142(2018):247-58.
16. Li T, Wang L. **Bending behavior of sandwich composite structures with tunable 3D-printed core materials**. Composite Structures;175(2017):46-57.
17. Sun Y, Guo L-c, Wang T-s, Zhong S-y, Pan H-z. **Bending behavior of composite sandwich structures with graded corrugated truss cores**. Composite Structures;185(2018):446-54.
18. Tonelli D, Bardella L, Minelli M. **A critical evaluation of mechanical models for sandwich beams**. Journal of Sandwich Structures & Materials;14(6)(2012):629-54.
19. Han SC, Lee JW, Kang K. **A New Type of Low Density Material: Shellular**. Advanced Materials;27(37)(2015):5506-11.
20. Abueidda DW, Bakir M, Abu Al-Rub RK, Bergström JS, Sobh NA, Jasiuk I. **Mechanical properties of 3D printed polymeric cellular materials with triply periodic minimal surface architectures**. Materials & Design;122(2017):255-67.
21. Qin Z, Jung GS, Kang MJ, Buehler MJ. **The mechanics and design of a lightweight three-dimensional graphene assembly**. Science Advances;3(1)(2017):e1601536.
22. Liu Y, Schaedler TA, Jacobsen AJ, Lu W, Qiao Y, Chen X. **Quasi-static crush behavior of hollow microtruss filled with NMF liquid**. Composite Structures;115(2014):29-40.
23. Zhou J, Deng X, Yan Y, Chen X, Liu Y. **Superelasticity and reversible energy absorption of polyurethane cellular structures with sand filler**. Composite Structures;131(2015):966-74.
24. Wang L, Lau J, Thomas EL, Boyce MC. **Co-Continuous Composite Materials for Stiffness, Strength, and Energy Dissipation**. Advanced Materials;23(13)(2011):1524-9.

25. Liu Y, Wang L. **Enhanced stiffness, strength and energy absorption for co-continuous composites with liquid filler**. Composite Structures;128(2015):274-83.
26. Harland D, Alshaer AW, Brooks H. **An Experimental and Numerical Investigation of a Novel 3D Printed Sandwich Material for Motorsport Applications**. Procedia Manufacturing;36(2019):11-8.
27. A. H. S, inventorInfinite Periodic Minimal Surfaces Without Self-Intersection. Washington, DC1970.
28. Yánez A, Cuadrado A, Martel O, Afonso H, Monopoli D. **Gyroid porous titanium structures: A versatile solution to be used as scaffolds in bone defect reconstruction**. Materials & Design;140(2018):21-9.
29. Yánez A, Herrera A, Martel O, Monopoli D, Afonso H. **Compressive behaviour of gyroid lattice structures for human cancellous bone implant applications**. Materials Science and Engineering: C;68(2016):445-8.
30. Carlsson LA, Kardomateas GA. Mechanics of Sandwich Composites Structural and Failure: Springer Dordrecht Heidelberg London New York; 2011.
31. EOS. PA2200 Material data sheet. 2019.
32. Stratasys. PolyJet Materials Data Sheet. In: Stratasys, editor. 2019.
33. Hutchinson JW, Suo Z. Mixed Mode Cracking in Layered Materials. In: Hutchinson JW, Wu TY, editors. Advances in Applied Mechanics. 29: Elsevier; 1991. p. 63-191.
34. La Magna R, Knippers J. Tailoring the Bending Behaviour of Material Patterns for the Induction of Double Curvature. In: De Rycke K, Gengnagel C, Baverel O, Burry J, Mueller C, Nguyen MM, et al., editors. Humanizing Digital Reality: Design Modelling Symposium Paris 2017. Singapore: Springer Singapore; 2018. p. 441-52.
35. Bilge K, Papila M. Interlayer toughening mechanisms of composite materials. In: Qin Q, Ye J, editors. Toughening Mechanisms in Composite Materials: Woodhead Publishing; 2015. p. 263-94.
36. Chandler DL. Researchers design one of the strongest, lightest materials known: MIT News; 2017 [Available from: https://news.mit.edu/2017/3-d-graphene-strongest-lightest-materials-0106.